ACS Catalysis

Research Article

pubs.acs.org/acscatalysis

Behavior of the Ru-bda Water Oxidation Catalyst Covalently Anchored on Glassy Carbon Electrodes

Roc Matheu,[†] Laia Francàs,[†] Petko Chernev,[‡] Mehmed Z. Ertem,[§] Victor Batista,[*,∥] Michael Haumann,[‡] Xavier Sala,[*,⊥] and Antoni Llobet[*,†,⊥]

[†]Institute of Chemical Research of Catalonia (ICIQ), Avinguda Països Catalans 16, 43007 Tarragona, Spain

[‡]Institut fur Experimentalphysik, Freie Universitat Berlin, Arnimallee 14, D-14195 Berlin, Germany

[§]Chemistry Department, Brookhaven National Laboratory, Upton, New York 11973, United States

[∥]Department of Chemistry, Yale University. P.O. Box 208107, New Haven, Connecticut 06520-8107, United States

[⊥]Departament de Química, Universitat Autònoma de Barcelona, Cerdanyola del Vallès, 08193 Barcelona, Spain

Supporting Information

ABSTRACT: Electrochemical reduction of the dizaonium complex, $[Ru^{II}(bda)(NO)(N{-}N_2)_2]^{3+}$, $\mathbf{2}^{3+}$ ($N{-}N_2^{2+}$ is 4-(pyridin-4-yl) benzenediazonium and bda^{2-} is 2,2′-bipyridine-6,6′-dicarboxylate), in acetone produces the covalent grafting of this molecular complex onto glassy carbon (GC) electrodes. Multiple cycling voltammetric experiments on the GC electrode generates hybrid materials labeled as **GC-4**, with the corresponding Ru-aqua complex anchored on the graphite surface. **GC-4** has been characterized at pH = 7.0 by electrochemical techniques and X-ray absorption spectroscopy (XAS) and has been shown to act as an active catalyst for the oxidation of water to dioxygen. This new hybrid material has a lower catalytic performance than its counterpart in homogeneous phase and progressively decomposes to form $\mathbf{RuO_2}$ at the electrode surface. Nevertheless the resulting metal oxide attached at the GC electrode surface, **GC-$\mathbf{RuO_2}$**, is a very fast and rugged heterogeneous water oxidation catalyst with TOF_is of 300 s^{-1} and TONs > 45 000. The observed performance is comparable to the best electrocatalysts reported so far, at neutral pH.

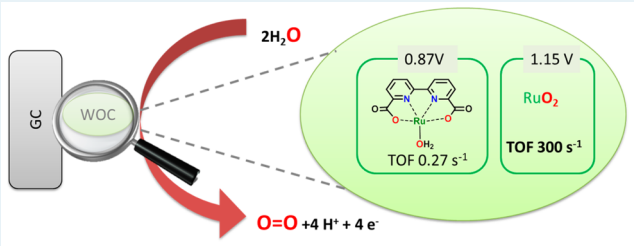

KEYWORDS: *water oxidation catalysis, electrocatalysis, water splitting, Ru complexes, modified graphite electrodes, heterogeneous water oxidation catalysis,* $\mathbf{RuO_2}$

1. INTRODUCTION

Catalytic water oxidation to molecular dioxygen is one of the key processes in photocatalytic cells that generate solar fuels by solar water-splitting.[1] In addition, the underlying four-electron/four-proton water oxidation is of biological interest since such reaction takes place at the oxygen-evolving Mn_4Ca complex of photosystem II in green plants and algae.[2]

Significant developments in the field of water oxidation catalysis have emerged over the past few years, including both molecular systems[3,4] and metal-oxide catalysts.[5−7] Water oxidation catalysts (WOCs) benefit from molecular toolkit that exploit electronic and steric effects and can be efficiently combined to generate extremely fast, oxidatively rugged catalysts.[8−16] For such purpose, the effects of ligand perturbations on catalyst performance need to be fully understood, including for example changes in ligand coordination modes, hydrogen-bonding, coordination numbers, inductive effects, and site isolation. Finally, molecular WOCs also benefit from an arsenal of spectroscopic techniques that can be applied to molecules and allow to derive detailed information on molecular and electronic structures.[17] In addition, anchoring WOCs on electrode surfaces is a very attractive strategy for generation of hybrid materials for heterogeneous water oxidation.[18−24]

Hybrid materials are very attractive since they can provide a large degree of flexibility to build photoelectrochemical cells for water splitting.[25−27] On the other hand, recent contributions have shown that metal oxides obtained from transition metal complexes exhibit highly active water oxidation catalysis. The nature of the transition metal complex as well as the oxide formation protocol strongly influence catalytic performance.[28,6,29,30]

$\mathbf{RuO_2}$ has long been known to be an effective electrocatalytic material for water oxidation to molecular dioxygen.[31,32] Recent work has focused on the relationship of particle size and shape with catalytic water oxidation performance, at different pHs, including catalysts immobilized on different electrode surfaces.[33−36] Here, we complement earlier studies by exploring the catalytic activation of graphite carbon electrodes by using the molecular Ru-aqua complex **GC-4** (see Scheme 1), obtained by

Received: January 22, 2015
Revised: April 20, 2015

DOI: 10.1021/acscatal.5b00132
ACS Catal. XXXX, XXX, XXX−XXX

Scheme 1. Synthetic Strategy Used for the Preparation of GC-4 Modified Electrodes[a]

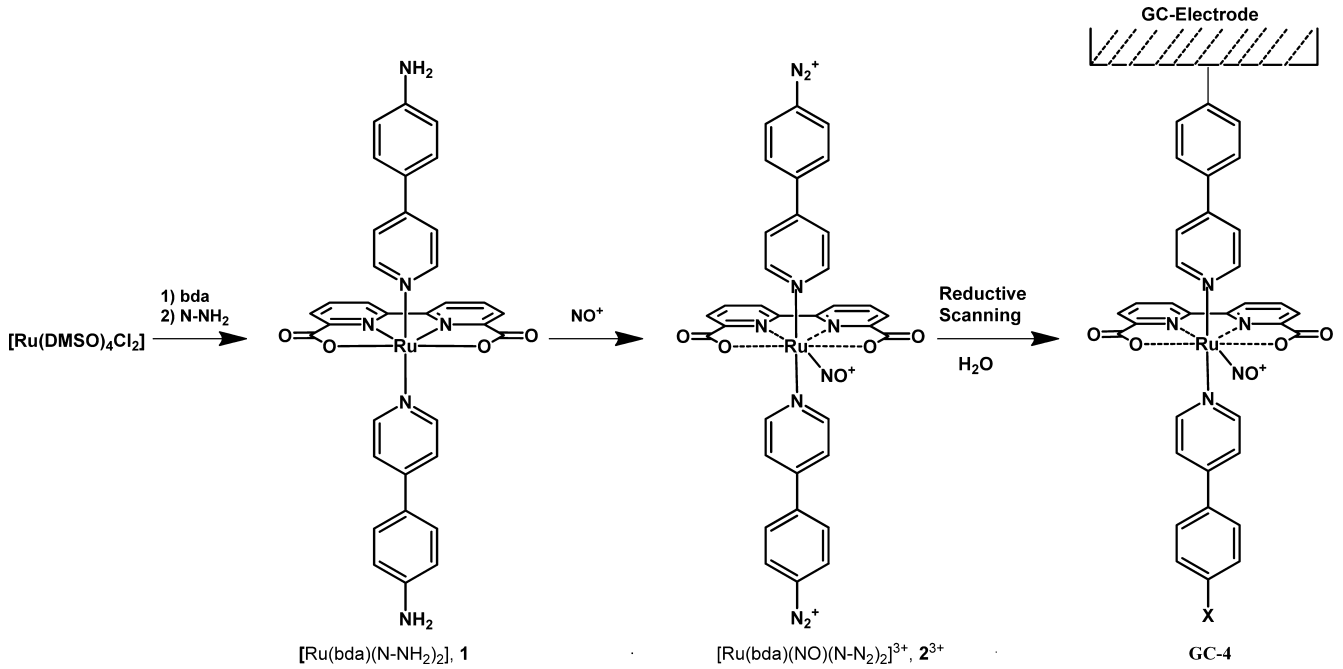

[a]bda^{2-} is [2,2′-bipyridine]-6,6′-dicarboxylate, N−NH_2 is 4-(pyridin-4-yl)aniline, and X = H and/or OH. The dashed lines at the first coordination sphere of the Ru metal center indicate bonds that are being simultaneously formed and broken.

reduction of the corresponding diazonium salt. Furthermore, we analyze the catalytic performance of these new hybrid materials with regard to water oxidation to molecular dioxygen reaction, and the fate of the Ru-complex precursor after catalytic performance.

2. RESULTS

2.1. Preparation and Electrochemical Anchoring of 2^{3+} into Graphitic Surfaces. The synthetic strategy followed for the preparation of glassy carbon electrodes modified with molecular Ru-bda (bda is [2,2′-bipyridine]-6,6′-dicarboxylate) based water oxidation catalysts is presented in Scheme 1. Reaction of $[Ru(DMSO)_4Cl_2]$, bda^{2-}, and 4-(pyridin-4-yl)-aniline (N−NH_2) generates the diamino complex $[Ru(bda)(N-NH_2)_2]$, **1**. Treatment of **1** with nitric oxide produces the oxidation of the amino groups to the corresponding highly reactive diazonium salts together with the formation of a Ru−NO group, generating $[Ru^{II}(bda)(NO)(N-N_2)_2]^{3+}$, 2^{3+}, as can be observed in Scheme 1. Complex 2^{3+} is then used as the starting material for the formation of hybrid materials upon electrochemical reduction of the diazonium derivatives. Complexes **1** and 2^{3+} were characterized by the usual analytic and spectroscopic techniques including NMR spectroscopy (see the SI) since both of them are diamagnetic.

The electrochemical properties of the complexes described in this work were investigated by means of cyclic voltammetry (CV). All the potentials are reported vs. SSCE unless explicitly stated otherwise. Reduction of the Ru-bda diazonium salt complex 2^{3+} on a glassy carbon electrode in acetone generates the hybrid material **GC-4X** (where X refers to a Ru vacant site where an acetone, or an aqua ligand can coordinate). This material in turn generates the Ru-aqua complex on the surface of the electrode, **GC-4** (see Scheme 1), upon several CV cycling experiments in a neat pH 7 phosphate buffer solution, as described below. The graphitic surfaces used to anchor the Ru complex 3^{2+} are depicted in Figure 1. Glassy carbon disks, **GC**, were used for the general evaluation of the redox properties of 2^{3+} and its surface anchored derivatives. Glassy carbon rods, **GCr**, were used because its high surface area allows to deposit very low concentrations of the active species. Glassy carbon thin plates, **GCp**, were used for synchrotron measurements and finally reticular vitreous carbon, commonly named "carbon sponge", **GCs**, were used for bulk electrolysis experiments because of their very high surface area.

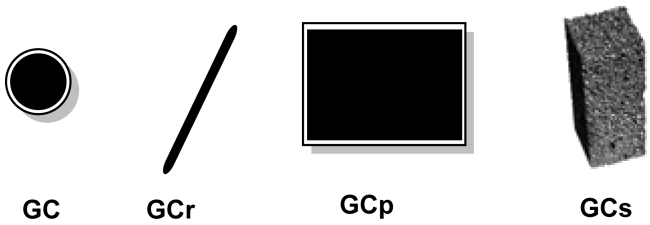

Figure 1. Drawing of working glassy carbon electrodes used in this work. Glassy carbon disk, **GC** (ϕ = 0.3 cm, S = 0.07 cm^2), glassy carbon rods, $\mathbf{GCr_x}$ (ϕ = 5 or 7 mm × 5 cm length and labeled $\mathbf{GCr_5}$ and $\mathbf{GCr_7}$, respectively), glassy carbon plates **GCp** (180 μm × 25 mm × 15 mm), and reticular vitreous carbon commonly named carbon sponge, $\mathbf{GC_s}$,(1 cm^3, S = 10 cm^2, 20 ppi). For the rotating disk electrode, a glassy carbon disk of ϕ = 0.4 cm (S = 0.125 cm^2) was used.

Figure 2 shows the electrochemical response obtained for 2^{3+} in acetone using a glassy carbon electrode disk (GC) of 0.07 cm^2 surface area. The scanning starts at 0.40 V toward the anodic region up to 0.80 V and then the potential is reversed at −0.40 V and swept back to 0.80 V. The large reductive irreversible wave at $E_{p,c}$ = 0.25 V (labeled 2 in Figure 2, left) is associated with the reduction of the diazonium group of 2^{3+} leading to a carbon radical generation, followed by C−C bond formation with the graphite electrode.[37,38] Depending on the

DOI: 10.1021/acscatal.5b00132
ACS Catal. XXXX, XXX, XXX−XXX

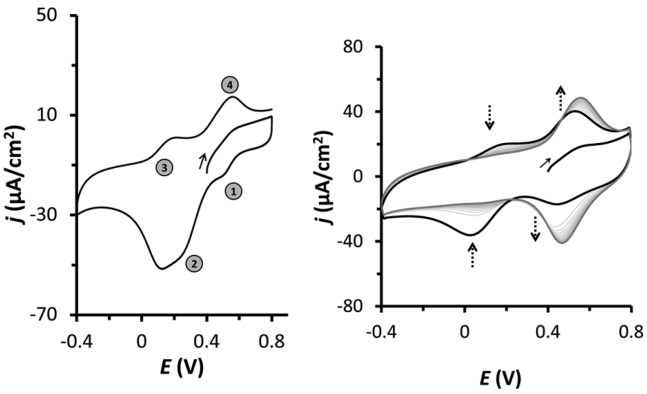

Figure 2. (left) Cyclic voltammetry showing the electrochemical response of $\mathbf{2}^{3+}$ dissolved in acetone, on a glassy carbon working electrode disk (see text for details). The solid arrow indicates the scan direction. Right, 20 repetitive cyclic voltammetric scans using **GC-4X** as the starting material in neat acetone, showing the disappearance of the wave due to the Ru−NO group at 0.15 V and the increase of the wave at 0.55 V (dashed arrows indicate increasing or decreasing current intensities upon scanning).

graphitic material, and given the axial nature of the two diazonium salts, the molecular complex can be anchored through any of the two sides. If only one side is anchored then one of the axial ligands will end up forming a terminal phenyl, or phenol group, or both.[37,38] From an electrochemical point of view, the activity of these complexes might be practically identical and thus will not be discriminated in the following.

The quasi-reversible wave at 0.15 V ($E_{p,a}$ = 0.20 V ; $E_{p,c}$ = 0.10 V; ΔE = 100 mV; labeled 3 in Figure 2) is associated with the one electron redox process of the nitrosyl group, both for the one just anchored on the glassy carbon electrode and the one that is in solution, associated with $\mathbf{2}^{3+}$. Finally the wave at 0.52 V ($E_{p,a}$ = 0.58 V; $E_{p,c}$ = 0.46 V; ΔE = 120 mV; labeled 1 and 4 in Figure 2) can be due to the oxidation of the initial complex ($\mathbf{2}^{3+}$) in solution as well as several Ru(III/II) processes of anchored species labeled **GC-4X** (X = acetone, water, NO or a vacant site) vide infra.

Because of the low stability of the nitrosyl group at low oxidation states under ambient light and high phosphate buffer concentrations,[39] the reduction wave at 0.15 V leads to the release of the nitrosyl group generating a vacant site. The latter can be potentially occupied by other coordinating molecules such as acetone or water depending on the conditions, as has also been observed for related Ru-NO complexes.[40,41] This can be clearly seen in Figure 2 (right), where a modified electrode generated in the same manner as in Figure 2 is transferred to a clean acetone solution with supporting electrolyte only. Upon 20 cycles from −0.40 to 0.80 the wave associated with the nitrosyl reduction diminishes whereas the wave associated with the **GC-4X**, III/II, process progressively increases. The direct interconversion is further corroborated by the fact that the overall charge at the cathodic III/II wave at the 20th cycle is practically the same as the sum of the initial III/II waves plus the one for the nitrosyl at the first scan. Alternatively, If **GC-4X** is cycled in a pH = 7 aqueous solution up to 1.2 V, the conversion from **GC-4X** to **GC-4** is much faster and with a single scan a complete conversion is obtained as shown in Figure S15 in the SI.

The amount of mass deposited on the electrode can be controlled by changing the applied potential, the time period for which this potential is applied, or the concentration of the initial diazonium salt $\mathbf{2}^{3+}$. Changing only initial concentration of the diazonium salt, while keeping the same protocol just described, provides an exquisite control of the mass deposited on the electrode surface (see the SI for further details).

2.2. Nature and Activity of the GC-4 Hybrid Materials at Low Potentials. The electrochemical properties of **GC-4** have been investigated by multiple scanning CV in water at pH 7.0, as displayed in Figure 3. The upper part of Figure 3 depicts

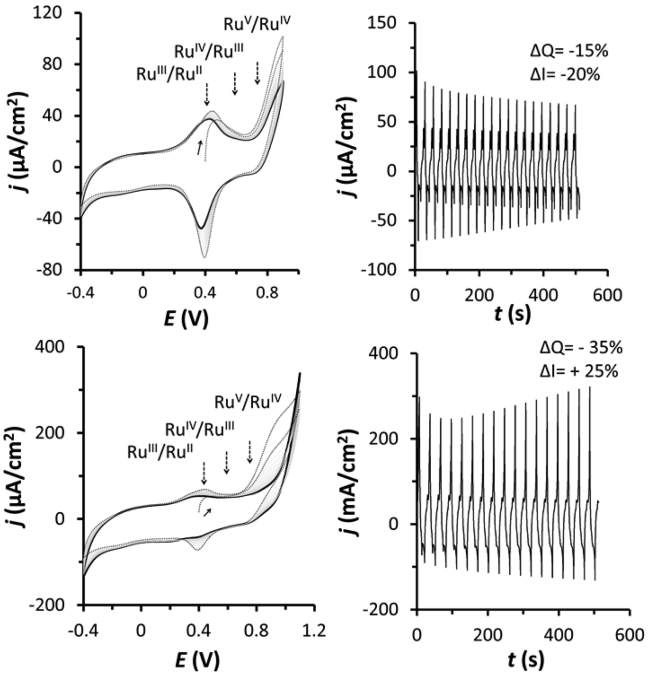

Figure 3. Cyclic voltammetry analysis of the electrocatalytic performance of **GC-4** at pH = 7.0 upon 20 repetitive scans up to 0.90 V (top) and up to 1.10 V (bottom). Solid arrows indicate the starting potential of the first cycle. The dashed line corresponds to the first cycle whereas the black line corresponds to the last one. In gray are depicted the rest of the cycles. ΔQ refers to the change of charge under the anodic wave at 0.50 V from the first to the last cycle. ΔI refers to the change of intensity of the anodic electrocatalytic wave at 0.90 V for the top experiments and at 1.10 V for the bottom. Dashed arrows indicate the redox couples of **GC-4** (Ru^{V}/Ru^{IV}, Ru^{IV}/Ru^{III}, and Ru^{III}/Ru^{II}).

the electrochemical performance of **GC-4** up to 0.90 V vs SSCE (all redox potentials reported in this work are versus the SSCE reference electrode unless explicitly mentioned) where the III/II couple at 0.40 V is clearly seen as well as the electrocatalytic wave associated with the V/IV couple that starts increasing its intensity at approximately 0.75 V. The IV/III couple that is located at 0.60 V is very weak as in the homogeneous phase probably due to slow proton coupled electron transfer process as has been observed for related Ru-aqua complexes.[42] The CV of **GC-4** nicely parallels that of $[Ru(bda)(4\text{-Me-py})_2]$[10] in the homogeneous phase at the same pH = 7 and thus corroborates the integrity of the molecular structure even when the complex is anchored on the surface.

Multiple scans, from −0.40 to 0.90, were carried out to evaluate the electrocatalytic performance of **GC-4** and its structural integrity. As can be observed in Figure 3 (top), for increasing number of cycles, the intensity of the catalytic wave decreases as well as the charge under the III/II wave. This observation suggests the presence of a deactivation pathway

DOI: 10.1021/acscatal.5b00132
ACS Catal. XXXX, XXX, XXX−XXX

that slowly reduces the performance of the **GC-4** material. Indeed, after 20 cycles, the charge below the III/II couple is reduced by 15% while the intensity of the electrocatalytic wave decreases by 20% of its initial value (the second cycle is always taken into consideration for these measurements). These experiments were also performed at 1.00, 1.10, and 1.20 V, as reported in Figure 3 (bottom) and Figures S17 and S18 (SI).

Chronoamperometric measurements were carried out at E_{app} = 0.87 V, allowing to calculate an indicative TOF of 0.27 s^{-1} assuming a 100% faradaic efficiency (see Figure S19). The approximate TOF_i compares well with that of a previously reported Ru-bda complex anchored on GC, following a related immobilization strategy.[22]

The multiple cycling performed at 1.10 V shows how the intensity of the III/II wave rapidly decreases after 20 cycles to approximately 35% of its original charge whereas, in sharp contrast now, the intensity at 1.10 V initially decreases but then rapidly increases by 25%. These phenomena are due to the depletion of the Ru−OH_2 active species from the surface of the electrode, concomitant with the generation of new species that are much more active than the Ru−OH_2 but shows a foot of the electrocatalytic wave that is anodically shifted to approximately 1.10 V. These new highly active species are due to the formation of **RuO_2** on the surface of the **GC** electrode, as will be demonstrated in the next section and will be labeled **GC-RuO_2** from now on throughout this manuscript. Interestingly, as is the case for most oxides,[5−7] the CV of the **GC-RuO_2** is featureless except for the electrocatalytic wave.

2.3. Nature and Activity of the GC-4 Hybrid Materials at High Potentials. We have anchored the Ru-aqua complex on large surface glassy carbon thin plates **GCp** (180 μm × 15 mm × 25 mm) to characterize the nature of the species on the electrode surface during catalytic turnover, following the evolution of reactive species by both electrochemistry and XAS. A similar protocol, as in the case of the **GC** electrodes, was employed here to generate the corresponding **GCp** hybrid materials.

Figure 4 shows the electrochemical activity of a **GCp-4X** material when exposed to 50 consecutive scans, from 0.00 to 1.20 V. The first scan mainly transforms **GCp-4X** into **GCp-4**. The increase of the anodic limit to 1.20 V increases the speed of the transformation of both **GCp-4X** into **GCp-4** and **GCp-4** into **GCp-RuO_2**. This observation is consistent with the featureless response of **GCp-RuO_2** except for the large electrocatalytic wave. Thus, the materials generated by electrooxidation involve a mixture of **GCp-4** and **GCp-RuO_2** with a relative composition that depends on the number of cycles. Furthermore, the absence of any other wave in the CV reveals the lack of intermediate species in this conversion, indicating a very fast and progressive transformation from **4** to **RuO_2** at the electrode surface. Figure 4 (top left) shows that the intensity under the III/II wave has decreased by about 50% after 25 cycles, suggesting that about half of the initial amount of **4** has been transformed into **RuO_2**.

Modified glassy carbon plates obtained at different voltammetric cycles, labeled **GCp-4_n** (n = 0, 5, 10, 25) where "n" indicates the number of cycles (Figure 4), were analyzed by XAS. The XAS results obtained for these four samples are summarized in Figure 5 and in the SI. After grafting complex $\mathbf{2}^{3+}$onto **GCp** electrodes, both the K-edge and EXAFS spectra of **GCp-4_0** indicated that the overall structure around the Ru center was preserved, although a slight increase of the Ru−N/O bond lengths was observed in **GCp-4_0** (Table S1). For

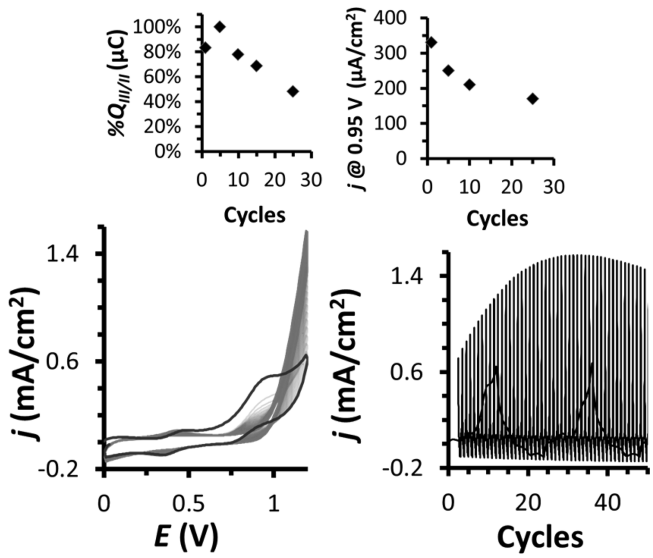

Figure 4. Repetitive cyclic voltammograms (50 cycles) for **GCp-4X** at pH = 7.0 up to 1.20 V. (bottom left) j vs E representation. The black solid line corresponds to the first cycle whereas the rest are drawn in gray. (bottom right) j vs E representation as a function of cycles. (top left) Plot of the charge under the anodic wave at 0.45 V upon cycling. (top right) Plot of current density at 0.95 V vs number of cycles (time).

increasing numbers of CV scans, an increase of the K-edge energy was observed (Figure 5B) and for **GCp-4_{25}** the increase was about ∼0.5 eV larger than for **GCp-4_0**. Assuming a K-edge shift of ∼1.7 eV per Ru oxidation step, our results suggests that ∼30% of the initial Ru(III) was oxidized to $Ru^{IV}O_2$. Further, EXAFS analysis revealed a slight decrease of the shorter Ru−N/O bond lengths in **GCp-4_n** for increasing CV scan numbers and an increase of the Fourier-Transform (FT) peaks around 3 Å. The ∼3 Å FT features and the corresponding EXAFS oscillations in the k-range of about 9−12 $Å^{-1}$ were similar to the spectral features of a **RuO_2** sample. Accordingly, EXAFS simulations yielded a new Ru−Ru distance of ∼3.6 Å which is similar to the Ru−Ru distance in **RuO_2** (see Table S1 in the SI). Such distance becomes more prominent for increasing numbers of CV scans (Figure 5D). The value of N_{Ru-Ru} of ∼1.3 suggests that ∼20% of the ruthenium in **GCp-4_{25}** is present in the form of **RuO_2**. The value obtained here for the transformation of **4** to **RuO_2** on the **GCp-4_{25}** electrode is substantially lower than the one obtained by CV probably due to the fact that not all the generated **RuO_2** remains tightly attached to the electrode surface and is partially washed off during the rinsing protocol used for the XAS sample preparation.

Further evidence for the formation of **RuO_2** comes from the XPS analysis of **GCr_7-4** and **GCr_7-RuO_2**, that contain basically the initial homogeneous catalyst anchored at a glassy carbon rod and **RuO_2** respectively (see section below for more details and the SI for the spectra). Indeed the signal associated with the N-1s region is practically at blank level in the **GCr_7-RuO_2** material, clearly indicating that the original ligands have disappeared.

2.4. Quantitative Analysis and Performance of Hybrid Materials for Catalytic Water Oxidation. The catalytic performance of **RuO_2**, electrodeposited on graphite electrodes by overoxidation of the molecular precursor **4**, was evaluated by CV and chronoamperometric methodologies. For such

DOI: 10.1021/acscatal.5b00132
ACS Catal. XXXX, XXX, XXX−XXX

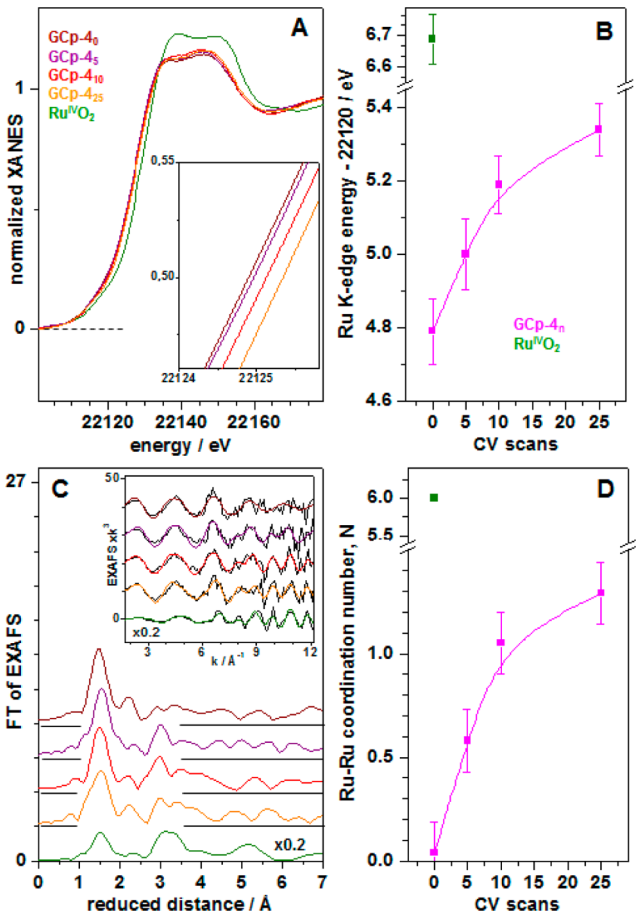

Figure 5. X-ray absorption spectroscopy analysis of **GCp-4$_n$** and **RuO$_2$**. (A) Ru K-edge spectra. (inset) Magnification of spectra around edge half-height. (B) Ru K-edge energies (determined at edge half-height). Error bars represent the accuracy of the energy calibration procedure. (C) FTs of EXAFS spectra. FTs were calculated for *k*-values of 1.7−12.2 Å^{-1} and using cos^2 windows extending over 10% at both *k*-range ends. Colors refer to the samples as indicated in part A; spectra were vertically shifted for comparison. (inset) EXAFS oscillations in *k*-space. Thin black lines are experimental data whereas thick (colored) lines are simulations using parameters shown in Table S1 in the SI. (D) Coordination number (*N*) of the Ru−Ru distance (~3.57 Å) of **RuO$_2$**, facilitating determination of the relative amounts of the oxide in the samples. Colors refer to samples as indicated in part B, error bars represent the approximate range of *N*-values obtained for using a Ru−Ru distance that was fixed to its value in **RuO$_2$** or (slightly) variable in the EXAFS simulations for **GCP-4$_n$**.

purpose, electrodeposition was performed on standard **GC** disk electrodes achieving surface concentrations close to a monolayer. **GC** rods of 5 and 7 mm diameter were also used to increase the surface area and to drastically decrease the amount of Ru complex anchored on the surface.

Initially, complex **2**$^{3+}$ was anchored on the **GC** or **GCr$_x$** (x = 5 or 7) electrodes, following the protocols as previously described. An adequate concentration of the complex was chosen to control the amount of deposited material. Then, the electrode surface was sonicated and rinsed with acetone and cleaned with a phosphate buffer solution at pH 7. Subsequently, the new material was scanned 3 times from −0.4 to 0.6 V in an aqueous solution at pH 7. The amount of the complex on the electrode surface was quantified by integrating the charge below the oxidative waves at 0.52 and 0.15 V. Finally, a potential of 1.20 V was applied for 6 min to ensure complete conversion from **GCr$_7$-4X** to **GCr$_7$-RuO$_2$**.

The catalytic activity of the new materials was analyzed by CV and chronoamperometry at pH 7.0. Figure 6 (left) shows

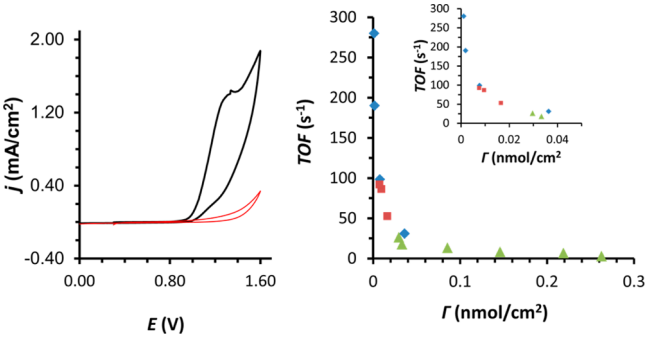

Figure 6. (left) Cyclic voltammetry of **GCr$_7$-RuO$_2$** with a superficial concentration of 25 pmols/cm^2 at pH = 7.0, showing a large electrocatalytic wave starting at 1.10 V (black line) and bare **GCr$_7$** at 20 mV/s of scan rate. (right) Plot of TOF for a series of **GCr$_7$-RuO$_2$** (blue diamonds), **GCr$_5$-RuO$_2$** (red squares), and **GC-RuO$_2$** (green triangles) and (inset) in the 0−0.05 nmol/cm^2 region. TOF are calculated from chronoamperometric experiments at 1.273 V (η = 0.70 V) for 360 s, after blank subtraction and assuming 100% Faradaic efficiency.

the CV of **GCr$_7$-RuO$_2$** with a surface concentration of 25 pmols/cm^2, exhibiting a huge electrocatalytic wave starting at 1.10 V that reaches impressive current densities above 1.5 mA/cm^2. Chronoamperometric experiments at E_{app} = 1.275 V (η = 0.70 V vs the 4e$^-$ oxidation of water to dioxygen, for 360 s) were used to calculate TOF$_i$. A plot of TOF$_i$ vs the **RuO$_2$** superficial concentration at the electrode is offered in Figure 6 (right), and a respective Tafel plot is in Figure S20. As it can be observed in Figure 6 (right), it is impressive to see the large increase of TOF$_i$ as the Γ decreases. In the particular case of **GCr$_7$-RuO$_2$** with Γ = 1.0 pmol, the TOF$_i$ reaches a value close to 300 Hz which is among the highest reported in the heterogeneous phase,[19,22−24] reaching values very similar to the best ones obtained so far in homogeneous phase.[10]

In order to be able to compare the performance of our electrode material with previous works reported in the literature for **RuO$_2$** and other oxides deposited at the surface of electrodes, we analyzed the roughness factor (RF) and the water oxidation catalytic activity following the benchmark proposed by Jaramillo et al.[43] A glassy carbon electrode disk (r = 0.20 cm) was used to analyze the double layer capacitance in the absence of faradaic processes to determine the electrochemically active surface area (ECSA) and RF; see Figure S21. Our experiments yielded an RF = 1−2 which indicates a surface coverage of **RuO$_2$** close or slightly above to one monolayer which is reasonable coming from a very small loading of the initial diazonium salt, **2**$^{3+}$. The estimation of the RF enabled us to obtain the specific current density, j_s, defined as the geometrical current density divided by RF. This parameter allows thus a fair comparison with other electrocatalytic materials since it takes into account the real surface area of the electrode. With regard to catalyst activity we carried out the test recommended by Jaramillo et al.[43] that consist on evaluating current densities (both j and j_s) as a function of potential using a rotating disk electrode (RDE) at 1600 rpm under 1 atm of O$_2$ under steady state conditions using the same

DOI: 10.1021/acscatal.5b00132
ACS Catal. XXXX, XXX, XXX−XXX

GC electrode, see Figure S22. Here our experiments show that to reach a j_s = 1 mA/cm^2 at pH = 7.0 an overpotential (η) of 0.65 V is needed. Under the same conditions the cobalt oxide water oxidation catalyst named "CoPi", that has been thoroughly studied,[44,45] needs η = 1.2 V at pH = 0 and η = 0.45 V at pH = 14. Under static conditions at pH = 7 CoPi needs η = 0.58 V to reach a j_s = 0.2 mA/cm^2,[46] whereas **GC-RuO$_2$** need only 0.50 V (see the Supporting Information section for additional details). The latter manifests that the **GC-RuO$_2$** electrode prepared in this work is among the best electrocatalytic materials reported so far.

Finally bulk electrolysis experiments were also carried out using high surface area reticulated carbon sponge electrodes **GCs** (20 ppi; volume = 1 cm^3). Following a similar protocol as for the carbon rod electrodes we generated **GCs-4** and **GCs-RuO$_2$**. The latter was used to carry out a bulk electrolysis experiment in a two compartment cell with an E_{app} = 1.15 V (η = 0.6 V) for 2 h containing a Clark electrode to measure the molecular oxygen generated in the gas phase. A plot of current intensity and [O$_2$] vs time is presented in Figure S23. It is impressive to see again that during the first 30 min TONs higher than 25 000 are achieved with basically 100% Faradaic efficiency. After 100 min the TON reaches a value of 45 000 although now the Faradaic efficiency drops, most likely due the oxidation of the carbon sponge electrode as has been observed before.[47]

3. DISCUSSION

3.1. Anchored WOCs and the Nature of Ru-bda on Graphitic Surfaces. Anchoring molecular WOCs on solid surfaces is an attractive strategy to generate hybrid solid-state materials that can be used to carry out heterogeneous water oxidation catalysis. Depending on the nature of the materials, water oxidation anodes or photoanodes can be built.[18−23,48,49] Anchored catalysts are very useful for building photoelectrochemical cells for water splitting since they provide a flexible engineering platform. However, one of the most challenging aspects is the proper characterization of the surface-immobilized species before, during, and after catalysis.

A number of WOCs have already been ***covalently*** anchored to metal-oxide surfaces, using carboxylate or phosphonate functionalities.[18−20] In addition, a few of them have been anchored on graphite surfaces.[22−24] The graphitic surfaces provide high conductivity, low-cost materials and are readily available in a myriad of conformations. In addition, invariably, every molecular water oxidation catalyst necessarily needs to cycle through a labile Ru−OH$_2$, or Ru−OH type of intermediate species. The oxide surfaces can potentially compete for this bond and thus generate Ru−O$_{surface}$ bonds that in turn deactivate the molecular catalyst. Such deactivation process does not occur on graphitic surfaces or to a much lesser extent in glassy carbon electrodes since the atomic ratio C/O is usually below 14%.[50] Therefore, from the functional perspective, GC surfaces might have advantages as solid supports when compared to metal-oxides. As a drawback, they are susceptible to oxidation under high applied potentials, so the graphitic surface can be oxidized and the C−C bond between the surface and the molecular catalyst can be broken. However, under "reasonable" potentials, the oxidation of the surface is negligible. In addition, new carbon-based materials such as the boron doped diamond (BDD)[51] or *nano*-ITO-reticulated vitreous carbon (*nano*-ITO-RVC)[52] are incredibly stable even at very high potentials.

Our strategy was to use diazonium salts attached to the axial ligands that basically maintain the intrinsic electronic properties of the metal center in the original complex. Upon controlled reduction, they readily attach to the surface of the electrode generating hybrid materials. CV, XPS, and especially XAS spectroscopy allows a thorough characterization of the nature of the anchored species, allowing for characterization of the fresh catalyst before turnover and for monitoring the fate of the catalyst under normal operating conditions.

3.2. Catalytic Performance of the Anchored Catalysts. At low potentials, up to the electrocatalytic wave, the **GC-4** behaves in a relatively discrete manner achieving TOF$_i$ of 0.27 s^{-1} at 0.87 V. After a few cycles, the catalyst slowly deactivates. This is in sharp contrast with the spectacular performance and stability of the catalyst in the homogeneous phase, where a TOF$_i$ close to 1000 Hz with an oxidative efficiency close to 100% is observed under optimized conditions using Ce(IV) as a primary oxidant.[15,16] The radically different behavior of the supported catalyst, when compared to the complex in solution, might be due to dimerization of the complex in the homogeneous phase upon reaching the high oxidation state Ru(V) to generate the RuOORu species via an I2M mechanism and subsequently dioxygen evolution.[10] The low translational mobility of the anchored Ru complex, due to the covalent C−C bond with the graphitic surface, precludes the dimer formation and favors the water nucleophilic attack type of mechanism. Such a process has higher activation energy and significant deactivation pathways, as judged by the loss of activity after a few catalytic cycles.

At higher potentials, the electrocatalytic wave shifts anodically by approximately 200 mV, indicating that a new material is formed while the original catalyst is depleted. Surprisingly, the newly generated material is extraordinarily active toward water oxidation. Such material is unambiguously characterized as a form of electrodeposited **RuO$_2$**. The transformation occurs without forming any detectable reaction intermediates, implying that it is rapidly completed through ligand degradation possibly all the way to CO$_2$.[53,54] The decomposition might happen in conjunction with ligand loss to the solution. Thus, the anchored molecular catalyst, for instance **GCr$_7$-4**, acts as a precursor for the generation of **RuO$_2$** electrodeposited on the electrode surface, forming **GCr$_7$-RuO$_2$**, with TOF$_i$ close to 300 s^{-1} and TONs > 45 000.

At this point, it is of interest to compare the activity of our materials to those that have already been reported in the literature. This is a very difficult task, due the different conditions under which the catalysts are described. To objectively evaluate the performance of the electrocatalytic materials, Jaramillo et al. have described benchmark tests that consists in calculating electroactive surface areas (ECSAs), roughness factors (RFs) and measurements of current densities (j and j_s) as a function of overpotential values.[43] Following this benchmark tests, a range of oxides including those of Co, Ni, and Ir have been evaluated at t pH = 0.0 and 14.0. These extreme conditions are needed to come up with the best performance for these oxides. Both at pH = 0 and pH = 14, IrOx turns out to be the best catalyst whereas CoPi performs relatively well at pH =14. Our catalyst exhibits high performance even at pH = 7.0, thus we compare our electrocatalytic materials with those of CoPi at pH = 7.0, for which the needed information is available.[46] The fact that our systems are comparable, or slightly better, in terms of specific current densities than those of CoPi manifests the excellent

DOI: 10.1021/acscatal.5b00132
ACS Catal. XXXX, XXX, XXX−XXX

performance for oxygen evolution of our hybrid electrocatalyst materials. In addition, while **GC-RuO$_2$** works in a neat pH = 7.0 electrolyte solution, the CoPi the systems need a 0.5 mM solution of Co(III) so that a significant amount of CoOx remains at the electrode.

Another interesting aspect of our system is the inverse correlation of the electrocatalytic activity versus surface concentration. This phenomenon has already been described for metal oxide nanoparticles (NP) and in particular for gold oxides NP[55] and has been ascribed to a combination of factors including electronic and geometrical effects.[55−57] From an electronic perspective, the smaller the particle (or nanoparticle) the higher the number of Ru atoms with low coordination sites. An additional influence to the performance can also be due to a synergistic interaction of the electrode surface and the catalyst NP as well as the superficial charge of the NP. From a geometrical perspective, different crystal facets can have different reactivity and the decrease of particle size can also generate an increase of these active facets with regard to the nonactive ones. In addition, NP can also have a certain degree of fluxionality that might influence performance. At present, we do not know which one of these factors and to what extend might be responsible for the inverse correlation. Further analysis of this aspect will be reported in the future.

4. CONCLUSIONS

We have synthesized Ru-bda complexes with axial pyridyl ligands, functionalized with diazonium salts that serve to attach the complexes to graphitic surfaces under reductive treatment. The resulting surface functionalization generates a solid-state material with modest catalytic activity. However, under performance conditions, it readily decomposes to form a highly dispersed **RuO$_2$** thin-film exhibiting outstanding electrocatalytic performance for electrocatalytic dioxygen evolution by water-splitting.

■ ASSOCIATED CONTENT

Supporting Information

The Supporting Information is available free of charge on the ACS Publications website at DOI: 10.1021/acscatal.5b00132.

Synthetic procedures and additional experimental, spectroscopic, and electrochemical data (PDF)

■ AUTHOR INFORMATION

Corresponding Authors

*E-mail: victor.batista@yale.edu (V.B.).
*E-mail: xavier.sala@uab.cat (X.S.).
*E-mail: allobet@iciq.es (A.L.).

Notes

The authors declare no competing financial interest.

■ ACKNOWLEDGMENTS

A.L. thanks MINECO (CTQ-2013-49075-R, SEV-2013-0319) and "La Caixa" foundation for financial support. R.M. thanks "La Caixa" foundation for a PhD grant. M.H. thanks the Deutsche Forschungsgemeinschaft for financial support (grant Ha3265/6-1) and for a Heisenberg Fellowship and the German Bundesministerium für Bildung und Forschung for funding within the Röntgen-Angström Cluster (grant 05K14KE1). We thank S. Reschke and M. Görlin for help in XAS data collection and M. Nachtegaal at SuperXAS of SLS for excellent technical support. M.Z.E. was funded by a Computational Materials and Chemical Sciences project at Brookhaven National Laboratory under contract DE-AC02-98CH10886 with the U.S. DOE. V.B. acknowledges supercomputer time from NERSC and financial support as part of the Argonne-Northwestern Solar Energy Research (ANSER) Center, an Energy Frontier Research Center funded by the U.S. Department of Energy, Office of Science, Office of Basic Energy Sciences under Award Number DE-SC0001059. X.S. thanks MINECO (CTQ2011-26440) for financial support.

■ REFERENCES

(1) *Molecular Water Oxidation Catalysis: A Key Topic for New Sustainable Energy Conversion Schemes*; Llobet, A., Ed.;John Wiley and Sons Ltd., 2014.

(2) Rappaport, F.; Guergova-Kuras, M.; Nixon, P. J.; Diner, B. A.; Lavergne, J. *Biochemistry* **2002**, *41*, 8518−8527.

(3) Singh, A.; Spiccia, L. *Coord. Chem. Rev.* **2013**, *257*, 2607−2622.

(4) Sala, X.; Maji, S.; Bofill, R.; Garcia-Anton, J.; Escriche, L.; Llobet, A. *Acc. Chem. Res.* **2014**, *47*, 504−516.

(5) Trotochaud, L.; Ranney, J. K.; Williams, K. N.; Boettcher, S. W. *J. Am. Chem. Soc.* **2012**, *134*, 17253−17261.

(6) Smith, R. D. L.; Prévot, M. S.; Fagan, R. D.; Zhang, Z.; Sedach, P. A.; Siu, M. K. J.; Trudel, S.; Berlinguette, C. P. *Science* **2013**, *340*, 60−63.

(7) Suntivich, J.; Gasteiger, H. A. *Nat. Chem.* **2011**, *3*, 546−550.

(8) Concepcion, J. J.; Tsai, M. K.; Muckerman, J. T.; Meyer, T. J. *J. Am. Chem. Soc.* **2010**, *132*, 1545−1557.

(9) Yin, Q.; Tan, J. M.; Besson, C.; Geletii, Y. V.; Musaev, D. G.; Kuznetsov, A. E.; Luo, Z.; Hardcastle, K. I.; Hill, C. L. *Science* **2010**, *328*, 342−345.

(10) Duan, L.; Bozoglian, F.; Mandal, S.; Stewart, B.; Privalov, T.; Llobet, A.; Sun, L. *Nat. Chem.* **2012**, *4*, 418−423.

(11) Karlsson, E. A.; Lee, B.-L.; Åkermark, T.; Johnston, E. V.; Kärkäs, M. D.; Sun, J.; Hansson, O.; Bäckvall, J.-E.; Åkermark, B. *Angew. Chem., Int. Ed.* **2011**, *50*, 11715−11718.

(12) Zhang, M.-T.; Chen, Z.; Kang, P.; Meyer, T. J. *J. Am. Chem. Soc.* **2013**, *135*, 2048−2051.

(13) Lopez, I.; Ertem, M. Z.; Maji, S.; Benet-Buchholz, J.; Keidel, A.; Kuhlmann, U.; Hildebrandt, P.; Cramer, C. J.; Batista, V. S.; Llobet, A. *Angew. Chem., Int. Ed.* **2014**, *53*, 205−209.

(14) Neudeck, S.; Maji, S.; Lopez, I.; Meyer, S.; Meyer, F.; Llobet, A. *J. Am. Chem. Soc.* **2014**, *136*, 24−27.

(15) Richmond, C. J.; Matheu, R.; Poater, A.; Falivene, L.; Benet-Buchholz, J.; Sala, X.; Cavallo, L.; Llobet, A. *Chem. - Eur. J.* **2014**, *20*, 17282−17286.

(16) Wang, L.; Duan, L.; Wang, Y.; Ahlquist, M. S. G.; Sun, L. *Chem. Commun.* **2014**, *50*, 12947−12950.

(17) See for instance: (a) Moonshiram, D.; Jurss, J. W.; Concepcion, J. J.; Zakharova, T.; Alperovich, I.; Meyer, T. J.; Pushkar, Y. *J. Am. Chem. Soc.* **2012**, *134*, 4625−4636. (b) Alperovich, I.; Moonshiram, D.; Concepcion, J. J.; Pushkar, Y. *J. Phys. Chem. C* **2013**, *117*, 18994−19001. (c) Stull, J. A.; Stich, T. A.; Hurst, J. K.; Britt, R. D. *Inorg. Chem.* **2013**, *52*, 4578−4586.

(18) Chen, Z.; Concepcion, J. J.; Jurss, J. W.; Meyer, T. J. *J. Am. Chem. Soc.* **2009**, *131*, 15580−15581.

(19) Ashford, D. L.; Lapides, A. M.; Vannucci, A. K.; Hanson, K.; Torelli, D. A.; Harrison, D. P.; Templeton, J. L.; Meyer, T. J. *J. Am. Chem. Soc.* **2014**, *136*, 6578−6581.

(20) Toma, F. M.; Sartorel, A.; Iurlo, M.; Carraro, M.; Parisse, P.; Maccato, C.; Rapino, S.; Gonzalez, B. R.; Amenitsch, H.; Da Ros, T.; Casalis, L.; Goldoni, A.; Marcaccio, M.; Scorrano, G.; Scoles, G.; Paolucci, F.; Prato, M.; Bonchio, M. *Nat. Chem.* **2010**, *2*, 826−831.

(21) Tong, L.; Gothelid, M.; Sun, L. *Chem. Commun.* **2012**, *48*, 10025−10027.

(22) Li, F.; Zhang, B.; Li, X.; Jiang, Y.; Chen, L.; Li, Y.; Sun, L. *Angew. Chem., Int. Ed.* **2011**, *50*, 12276−12279.

DOI: 10.1021/acscatal.5b00132
ACS Catal. XXXX, XXX, XXX−XXX

(23) Mola, J.; Mas-Marza, E.; Sala, X.; Romero, I.; Rodríguez, M.; Viñas, C.; Parella, T.; Llobet, A. *Angew. Chem., Int. Ed.* **2008**, *47*, 5830−5832.
(24) deKrafft, K. E.; Wang, C.; Xie, Z.; Su, X.; Hinds, B. J.; Lin, W. *ACS Appl. Mater. Interfaces* **2012**, *4*, 608−613.
(25) Hambourger, M.; Gervaldo, M.; Svedruzic, D.; King, P. W.; Gust, D.; Ghirardi, M.; Moore, A. L.; Moore, T. A. *J. Am. Chem. Soc.* **2008**, *130*, 2015−2022.
(26) Youngblood, W. J.; Lee, S.-Y. A.; Kobayashi, Y.; Hernandez-Pagan, E. A.; Hoertz, P. G.; Moore, T. A.; Moore, A. L.; Gust, D.; Mallouk, T. E. *J. Am. Chem. Soc.* **2009**, *131*, 926−927.
(27) Li, L.; Duan, L.; Xu, Y.; Gorlov, M.; Hagfeldt, A. S.; Sun, L. *Chem. Commun.* **2010**, *46*, 7307−7309.
(28) Wang, D.; Ghirlanda, G.; Allen, J. P. *J. Am. Chem. Soc.* **2014**, *136*, 10198−10201.
(29) Hong, D.; Jung, J.; Park, J.; Yamada, Y.; Suenobu, T.; Lee, Y.-M.; Nam, W.; Fukuzumi, S. *Energy Environ. Sci.* **2012**, *5*, 7606−7616.
(30) Chen, G.; Chen, L.; Ng, S.-M.; Lau, T.-C. *ChemSusChem* **2014**, *7*, 127−134.
(31) Harriman, A.; Pickering, I. J.; Thomas, J. M.; Christensen, P. A. *J. Chem. Soc., Faraday Trans. 1* **1988**, *84*, 2795.
(32) Over, H. *Chem. Rev.* **2012**, *112*, 3356.
(33) Zhang, Y.; Judkins, E. C.; McMillin, D. R.; Mehta, D.; Ren, T. *ACS Catal.* **2013**, *3*, 2474.
(34) Zhang, Y.; Ren, T. *Chem. Commun.* **2012**, *48*, 11005.
(35) Okeyoshi, K.; Yoshida, R. *Adv. Funct. Mater.* **2010**, *20*, 708.
(36) Lee, Y.; Suntivich, J.; May, K. J.; Perry, E. E.; Shao-Horn, Y. *J. Phys. Chem. Lett.* **2012**, *3*, 399.
(37) Belanger, D.; Pinson, J. *Chem. Soc. Rev.* **2011**, *40*, 3995−4048.
(38) Pinson, J.; Podvorica, F. *Chem. Soc. Rev.* **2005**, *34*, 429−439.
(39) Gomes, A. J.; Espreafico, E. M.; Tfouni, E. *Mol. Pharmaceutics* **2013**, *10*, 3544−3554.
(40) Roveda, A. C., Jr.; Bueno-Ruiz-Papa, T.; Castellano, E. E.; Wagner-Franco, D. *Inorg. Chim. Acta* **2014**, *409*, 147−155.
(41) Doro, F. G.; Rodrigues-Filho, U. P.; Tfouni, E. *J. Colloid Interface Sci.* **2007**, *307*, 405−417.
(42) Llobet, A.; Doppelt, P.; Meyer, T. J. *Inorg. Chem.* **1988**, *27*, 514−520.
(43) McCrory, C. C. L.; Jung, S.; Peters, J. C.; Jaramillo, T. F. *J. Am. Chem. Soc.* **2013**, *135*, 16977−16987.
(44) Other metal oxides behaved similarly, e.g, CoOx, CoFeOx, NiOx, showing an overpotential between 0.3 and 0.5 V at pH = 14 and between 0.8 and 1.2 V at pH = 0 in ref 42.
(45) IrO_2 oxide nanoparticled behaved better than other oxides at pH = 0 with an overpotential of 0.3 V at pH = 0 as described in ref 38.
(46) Kanan, M. W.; Nocera, D. G. *Science* **2008**, *321*, 1072−1075.
(47) Barnett, S. M.; Goldberg, K. I.; Mayer, J. M. *Nat. Chem.* **2012**, *4*, 498−502.
(48) Vannucci, A. K.; Alibabaei, L.; Losego, M. D.; Concepcion, J. J.; Kalanyan, B.; Parsons, G. N.; Meyer, T. J. *Proc. Natl. Acad. Sci. U. S. A.* **2013**, *110*, 20918−20922.
(49) Gao, Y.; Ding, X.; Liu, J.; Wang, L.; Lu, Z.; Li, L.; Sun, L. *J. Am. Chem. Soc.* **2013**, *135*, 4219−4222.
(50) McCreery, L. R. *Chem. Rev.* **2008**, *108*, 2646−2687.
(51) McCreery, R. L. *Chem. Rev.* **2008**, *108*, 2646−2687.
(52) Méndez, M. A.; Alibabaei, L.; Concepcion, J. J.; Meyer, T. J. *ACS Catal.* **2013**, *3*, 1850−1854.
(53) Francas, L.; Sala, X.; Escudero-Adan, E.; Benet-Buchholz, J.; Escriche, L.; Llobet, A. *Inorg. Chem.* **2011**, *50*, 2771−2781.
(54) Hong, D.; Mandal, S.; Yamada, Y.; Lee, Y.-M.; Nam, W.; Llobet, A.; Fukuzumi, S. *Inorg. Chem.* **2013**, *52*, 9522−9531.
(55) Carchini, G.; Almora-Barrios, N.; Revilla-López, G.; Bellarosa, L.; García-Muelas, R.; García-Melchor, M.; Pogodin, S.; Błoński, P.; López, N. *Top. Catal.* **2013**, *56*, 1262−1272.
(56) Valden, M.; Lai, X.; Goodman, D. W. *Science* **1998**, *281*, 1647−1650.
(57) Xhou, Z.; Flytzani-Stephanopoulos, M.; Saltsburg, H. *J. Catal.* **2011**, *280*, 255−263.

DOI: 10.1021/acscatal.5b00132
ACS Catal. XXXX, XXX, XXX−XXX